Electronic Supplementary Material (ESI) for Catalysis Science & Technology.


**Electronic Supporting Information**

# A two-dimensional Ni(II) coordination polymer based on 3,5-bis(1',2',4'-triazol-1'-yl) pyridine ligand for water electro-oxidation

Chun-Ling Wang[1], Chuan-Qi Song[1], Wen-Hui Shen, Yuan-Yuan Qi,
Ying Xue, Yao-Cheng Shi*, Huaguang Yu*, Ligang Feng*

College of Physics Science and Technology, and College of Chemistry and Chemical Engineering, Yangzhou University, Yangzhou 225002, P. R. China

Email addresses:
ycshi@yzu.edu.cn (Y Shi), hgyu@yzu.edu.cn (H Yu), ligang.feng@yzu.edu.cn (L Feng)

1 These authors contributed equally to this work.

## 1. Material and methods

Nickel nitrate ($Ni(NO_3)_2 \cdot 6H_2O$), benzene-1,3,5-tricarboxylic acid ($C_9H_6O_7$), 3,5-dibromopyridine ($C_5H_3Br_2N$), copper oxide (CuO), 1,2,4-triazole ($C_2H_3N_3$), potassium carbonate ($K_2CO_3$) and potassium hydroxide (KOH) were purchased from Sinopharm Chemical Reagent Corporation. $^1H$ and $^{13}C$ nuclear magnetic resonance (NMR) spectra were recorded on a Bruker AVANCE 600 spectrometer. The electrospray ionization mass spectrum (ESI-MS) was collected on a Bruker maXis mass spectrometer. Fourier transform infrared spectroscopy (FT-IR) data were collected using a Bruker Tensor 27 FTIR spectrometer. Elemental analyses (C, H, and N) were carried out on an Elementar vario EL cube elemental analyzer. Thermal gravimetric analysis (TGA) was carried out using a PerkinElmer Pyris 1 TGA under a constant stream of dry nitrogen gas (flow rate 20 mL $min^{-1}$) over the temperature range 30-900℃ and at a heating rate of 10 K $min^{-1}$. Phase purity was confirmed using a Shimadzu XRD-7000 powder X-ray diffractometer with Cu Kα radiation (the X-ray generator operating at 40 kV and 30 mA) and a Ni monochromator. The data were collected in the range of 5-60° with a step size of 0.02° and a count rate of 2.0° $min^{-1}$. All the electrochemical measurements were performed with a Bio-Logic VSP (Bio-Logic Co., France). The surface chemical compositions and electronic states of the samples before and after OER test were probed by a ThermoFisher Scientific ESCALAB 250Xi X-ray Photoelectron Spectrometer (XPS). High-resolution TEM (HRTEM) images were captured on the FEI Tecnai G2 F30 S-TWIN (USA).

## 2. Synthesis of 3,5-bis(1',2',4'-triazol-1'-yl) pyridine ligand 1

The solution of 3,5-dibromopyridine (26.8 g, 113 mmol), 1,2,4-triazole (19.5 g, 283 mmol), copper(II) oxide (2.19 g, 28.3 mmol), potassium carbonate (39.1 g, 283 mmol), and DMSO (150 mL) was heated at 150℃ for 48 h. After cooling to room temperature, the mixture was diluted with 1.5 L $CH_2Cl_2$, and then filtered through a column of basic alumina. The filtrate was washed with $CH_2Cl_2$ (500 mL). $CH_2Cl_2$ was distilled off by rotary evaporation, and a yellow oil liquid was obtained. Saturated NaCl solution was added to it, and a white solid was precipitated. The mixture was filtered through a Buchner funnel and washed with distilled water for three times. After drying in vacuum an off-white solid was got (19 g, 79 %).

## 3. Synthesis of Ni(II) coordination polymer 2

A mixture containing $Ni(NO_3)_2 \cdot 6H_2O$ (43.6 mg, 0.15 mmol), benzene-1,3,5-tricarboxylic acid (10.5 mg, 0.05 mmol), and 3,5-bis(1',2',4'-triazol-1'-yl) pyridine (21.3 mg, 0.10 mmol) in 5 mL $H_2O$ was sealed in a 25 mL Teflon® reactor, which was heated at 120℃ for 3 days. After being cooled to room temperature, block green crystals of Ni-CP were obtained in about 50 % yield (based on 3,5-bis(1',2',4'-triazol-1'-yl) pyridine). Elemental alal. Found: C, 33.25; H, 3.96; N, 14.89 %. Calc. for $C_{36}H_{40}N_{14}Ni_3O_{22} \cdot 6H_2O$: C, 33.13; H, 4.02; N, 15.03 %.

## 4. Structure determination of single crystals

Suitable single crystals of **1** and **2** were selected for single crystal X-ray diffraction. Crystallographic data were collected on a Bruker AXS D8 ADVANCE single crystal X-ray diffractometer with graphite monochromated Mo Kα radiation (λ= 0.71073 Å). The APEX 3 program was used to collect frames of data, index the reflections and determine the lattice parameters; SAINT [1] was used for the integration of the intensity of the reflections and scaling; SADABS [2] was used for absorption correction; and SHELXTL [3, 4] was used for space-group determinations. The structure was solved by direct methods with SHELXT program [5] and refined by full matrix least-square methods on the basis of $F^2$ using SHELXL-2014 program [6, 7] contained in OLEX2 suite graphical user interface [8]. The contribution of the disordered solvent molecules to the diffraction pattern could not be rigorously included in the model and was consequently removed with the SQUEEZE routine [9] of PLATON [10] or with the mask tool implemented in OLEX2. All non-hydrogen atoms were refined with anisotropic displacement parameters during the final cycles. All hydrogen atoms of the organic molecule were placed by geometrical considerations and were added to the structure factor calculation. The crystallographic information files (CIFs) were compiled with OLEX2. The program PLATON enabled checking for additional symmetry elements. The overall structure of the Ni(II) coordination polymer **2** is a 2D (2,3)-connected framework with the point symbol of $(12^3)_2(12)_3$ topology, as analyzed by TOPOS software [11]. A summary of the crystallographic data for compounds 1 and 2 is listed in Table S1. Crystallographic figures were generated with the Diamond 3.1e software [12]. CCDC 1856011 (for **1**) and 1856012 (for **2**) contain the supplementary crystallographic data for this paper. These data can be obtained free of charge from The Cambridge Crystallographic Data Centre.

## 5. The electrochemical catalytic activity of the Ni(II) coordination polymer

The powders were finely ground before use. Ni-CP/C inks were prepared by dispersing 2.5 mg of catalyst materials (consisting of Ni-CP and carbon black) in 475 μL of ethanol ($C_2H_5OH$) with 25μL of 5 wt% Nafion® solution and then sonicated (for 30 min) until homogeneous inks were formed. Then 5μL of the catalyst ink was drop-cast on glassy carbon electrodes (GCEs) with the same loading of 0.35 mg $cm^{-2}$ and dried at room temperature. The electrochemical tests were implemented on a Bio-Logic SAS VSP electrochemical workstation using a three-electrode system. Ni-CP/C modified GCEs (geometric area: 0.07 $cm^2$) were used as the working electrode in 1.0 M KOH solution, a Pt plate as the counter electrode, and a saturated calomel electrode (SCE) was used as the reference electrode and it was calibrated before and after the electrochemical test to make sure the accuracy. All of the potentials measured in this case were converted to the reversible hydrogen electrode (RHE) based on the equation $E_{RHE} = E_{SCE} + 0.0591\ pH + 0.242\ V$. The electrode was initially activated at a sweep rate of 20 mV $s^{-1}$ for 40 cycles to yield a stable voltammetric response. The electrochemical impedance spectroscopy (EIS) was recorded in the above three-electrode cell at room temperature in 1M KOH. The frequency varied from 1MHz to 0.1 Hz and the amplitude of the sinusoidal potential signal was 5 mV. The chronoamperometry (CA) was measured in 1M KOH at the overpotential of 0.386 V for 12h. The turnover frequency (TOF, defined as mol $O_2$ per mol metal per second) was evaluated by the following equation [13]

$$TOF=\frac{j\times A}{4\times m\times F} \qquad (1)$$

where, *j* is the current density at an overpotential of 0.4 V. *A* and m are the area of the electrode and the number of moles of the active materials that were deposited onto the electrode, respectively. F is the Faraday constant (96485 C $mol^{-1}$).

Table S1: Crystallographic data and structure refinement parameters for compounds **1** and **2**

| Compound | **1** | **2** |
|---|---|---|
| Empirical formula | $C_9H_7N_7 \cdot H_2O$ | $C_{36}H_{40}N_{14}Ni_3O_{22}$ |
| Formula weight | 231.23 | 1196.95 |
| Temperature (K) | 295(2) | 295(2) |
| Crystal system | orthorhombic | monoclinic |
| Space group | *P*na2$_1$ (no. 33) | *C*2/*c* (no. 15) |
| a (Å) | 12.569(2) | 20.1497(19) |
| b (Å) | 22.176(3) | 7.1876(7) |
| c (Å) | 3.6728(6) | 34.937(4) |
| α (°) | 90.00 | 90.00 |
| β (°) | 90.00 | 94.669(3) |
| γ (°) | 90.00 | 90.00 |
| Volume (Å$^3$) | 1023.7(3) | 5043.0(9) |
| Z | 4 | 4 |
| Density (calc.) (g cm$^{-3}$) | 1.500 | 1.577 |
| λ (Mo Kα) (Å) | 0.71073 | 0.71073 |
| Absorption coefficient (μ mm$^{-1}$) | 0.109 | 1.201 |
| *F* (000) | 480.0 | 2456.0 |
| $2\theta_{max}$ (°) | 55 | 55 |
| Goodness-of-fit on $F^2$ | 1.061 | 1.032 |
| $R_{int}$ | 0.0445 | 0.0508 |
| $R_1/wR_2$ ($I > 2\sigma(I)$) [a] | 0.0366, 0.0800 | 0.0483, 0.1178 |
| $R_1/wR_2$ (all data) | 0.0478, 0.0865 | 0.0852, 0.1319 |

[a] $\mathbf{R_1}=\frac{\sum||F_o|-|F_c||}{\sum|F_o|}$; $\mathbf{wR_2}=\left[\frac{\sum w\left(F_o^2-F_c^2\right)^2}{\sum w\left(F_o^2\right)^2}\right]^{1/2}$

Table S2: Selected bond lengths (Å) for the Ni(II) coordination polymer

| bond | Length(Å) | bond | Length(Å) |
|---|---|---|---|
| Ni1-N1 | 2.107(3) | Ni2-N6 | 2.078(3) |
| Ni1-N1#2 [a] | 2.107(3) | Ni2-N4#1 [a] | 2.117(3) |
| Ni1-O1 | 2.074(3) | Ni2-O3 | 2.072(3) |
| Ni1-O1#2 [a] | 2.074(3) | Ni2-O4 | 2.063(3) |
| Ni1-O2 | 2.041(3) | Ni2-O5 | 2.078(3) |
| Ni1-O2#2 [a] | 2.041(3) | Ni2-O6 | 2.064(2) |
| | | N4-Ni2#3 [a] | 2.117(3) |

[a] #1: 1/2 - X, 1/2 + Y, 1/2 - Z; #2: 1 - X, - 1 - Y, 1 - Z; #3: 1/2 - X, - 1/2 + Y, 1/2 - Z.

Table S3: Selected angles (°) for the Ni(II) coordination polymer

| angle | (°) | angle | (°) |
|---|---|---|---|
| N1-Ni1-N1#2 [a] | 180.00(16) | O6-Ni2-N6 | 87.74(10) |
| O2-Ni1-N1#2 [a] | 88.94(11) | O6-Ni2-N4#1 [a] | 178.03(11) |
| O2#2-Ni1-N1 [a] | 88.94(11) | O6-Ni2-O5 | 91.76(10) |
| O2-Ni1-N1 | 91.06(11) | N6-Ni2-N4#1 [a] | 92.36(10) |
| O2#2-Ni1-N1#2 [a] | 91.06(11) | O3-Ni2-O6 | 87.68(11) |
| O2-Ni1-O2#2 [a] | 180.00 | O3-Ni2-N6 | 93.01(12) |
| O2#2-Ni1-O1 [a] | 87.82(12) | O3-Ni2-N4#1 [a] | 90.35(11) |
| O2#2-Ni1-O1#2 [a] | 92.18(12) | O3-Ni2-O5 | 179.42(12) |
| O2-Ni1-O1 | 92.18(12) | O3-Ni2-O4 | 89.46(13) |
| O2-Ni1-O1#2 [a] | 87.82(12) | O5-Ni2-N6 | 87.12(12) |
| O1-Ni1-N1#2 [a] | 90.82(11) | O5-Ni2-N4#1 [a] | 90.21(11) |
| O1#2-Ni1-N1#2 [a] | 89.18(11) | O4-Ni2-O6 | 90.35(10) |
| O1#2-Ni1-N1 [a] | 90.82(11) | O4-Ni2-N6 | 176.81(12) |
| O1-Ni1-N1 | 89.18(11) | O4-Ni2-N4#1 [a] | 89.64(11) |
| O1#2-Ni1-O1 [a] | 180.0 | O4-Ni2-O5 | 90.39(13) |

[a] #1: 1/2 - X, 1/2 + Y, 1/2 - Z; #2: 1 - X, - 1 - Y, 1 - Z; #3: 1/2 -X, - 1/2 + Y, 1/2 - Z.

Table S4: OER activity comparison to analogous MOF or CP electrocatalysts

| materials | electrolytes | substrates | η (V) | j (mA $cm^{-2}$) | TOF [a] ($s^{-1}$) | refs |
|---|---|---|---|---|---|---|
| Ni-CP/C 1: 2 | 1.0 M KOH | glassy carbon | 0.356 | 10 | 0.21@ 0.4 V | this work |
| NiFe-MOF | 0.1 M KOH | glassy carbon | 0.406 | 10 | | [14] |
| Co-ZIF-9 | 0.1 M $K_3PO_4$ buffer(pH = 7.0) | FTO glass | 0.510 | 1 | 0.0017 6 | [15] |
| $[Co_2(\mu\text{-}Cl)_2(btta)]$ | 1.0 M KOH | glassy carbon | 0.508 | 10 | | [16] |
| $[Co_2(\mu\text{-}OH)_2(btta)]$ | 1.0 M KOH | glassy carbon | 0.387 | 10 | | [16] |
| $Co(bpamb)_{0.5}(adip)$ | 0.2 M $K_3PO_4$ buffer(pH = 6.8) | glassy carbon | 0.46 | | | [17] |
| $Fe_3$-BPTC(NNU-21) | 0.1 M KOH | carbon cloth | 0.555 | 10 | | [18] |
| $Fe_2Co$-BPTC (NNU-22) | 0.1 M KOH | carbon cloth | 0.376 | 10 | | [18] |
| $Fe_2Ni$-BPTC (NNU-23) | 0.1 M KOH | carbon cloth | 0.365 | 10 | | [18] |
| $Fe_2Zn$-BPTC (NNU-24) | 0.1 M KOH | carbon cloth | 0.522 | 10 | | [18] |
| UTSA-16 | 1.0 M KOH | glassy carbon | 0.408 | 10 | | [19] |

[a] @an overpotential.

Table S5: The detailed EIS data of Ni-CP, Ni-CP/C 1: 1, Ni-CP/C 1: 2 and Ni-CP/C 1:3

| Samples | Rs [a] | $R_{ct}$ [b] | CPE [c] | n [d] | $R_1$ [e] | $CPE_1$ [f] | n [d] |
|---|---|---|---|---|---|---|---|
| | Ω | Ω | S $s^{-n}$ | 0<n<1 | Ω | S $s^{-n}$ | 0<n<1 |
| Ni-CP | 8.651 | 235.9 | $8.217E^{-5}$ | 0.8310 | 0.4994 | $9.107E^{-5}$ | 0.9600 |
| Ni-CP/C 1:1 | 6.739 | 40.26 | $3.784E^{-4}$ | 0.8773 | 22.89 | $3.193E^{-2}$ | 0.3312 |
| Ni-CP/C 1:2 | 9.277 | 20.54 | $1.802E^{-3}$ | 0.8135 | 10.31 | $2.825E^{-2}$ | 0.3480 |
| Ni-CP/C 1:3 | 8.903 | 94.16 | $9.757E^{-5}$ | 0.8720 | 1.825 | $3.399E^{-4}$ | 0.6896 |

[a] solution resistance;
[b] interfacial charge transfer resistance;
[c] interfacial charge capacitance;
[d] which represents the deviation from the ideal behaviour, being n = 1 for perfect capacitors;
[e] adsorption resistance;
[f] adsorption charge capacitance.

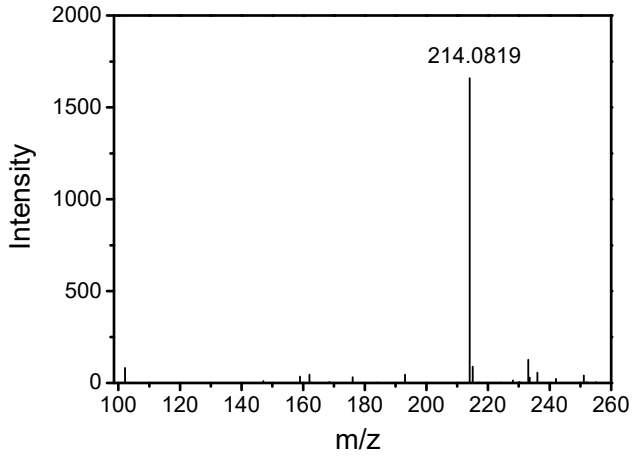


Figure S1: ESI-MS(+) spectra of 3,5-bis(1',2',4'-triazol-1'-yl) pyridine

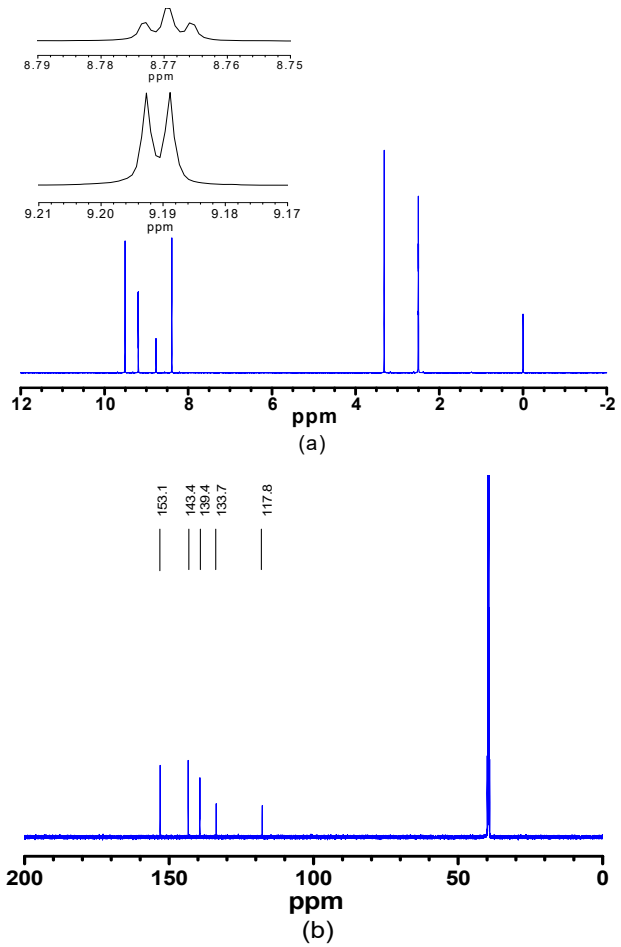


Figure S2: (a) $^{1}$H and (b) $^{13}$C NMR spectra of 3,5-bis(1',2',4'-triazol-1'-yl) pyridine in DMSO-$d_6$.

$^{1}$H NMR (DMSO-$d_6$, 600.2 MHz): δ 9.5 (s, 2H), 9.2 (d, $J$ =2.3 Hz, 2H), 8.8 (t, $J$ = 2.2 Hz, 1H), 8.4 (s, 2H). $^{13}$C NMR (DMSO-$d_6$,150.9 MHz): δ 153.1, 143.4, 139.4, 133.7, 117.8.

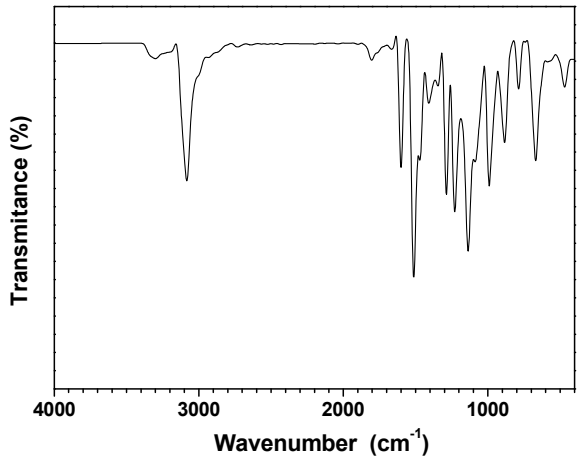


Figure S3: FT-IR spectrum of 3,5-bis(1',2',4'-triazol-1'-yl) pyridine.

FT-IR (KBr pellet, $cm^{-1}$): 3078 (m), 1811 (w), 1596 (m), 1516 (s), 1412 (w), 1340 (w), 1284 (m), 1221 (s), 1133 (s), 982 (m), 886 (m), 790 (w), 663 (m), 471 (w). The bands at 1800-1100 $cm^{-1}$ are ascribed to stretching vibrations of $\nu_{as}$(C=C), $\nu_{as}$ (C=O), $\nu_{as}$ (C=N) and $\nu_{as}$ (N=N).

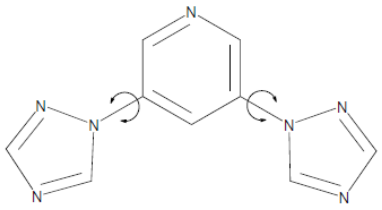

Figure S4: The structure and conformations of 3,5-bis(1’,2’,4’-triazol-1’-yl) pyridine.

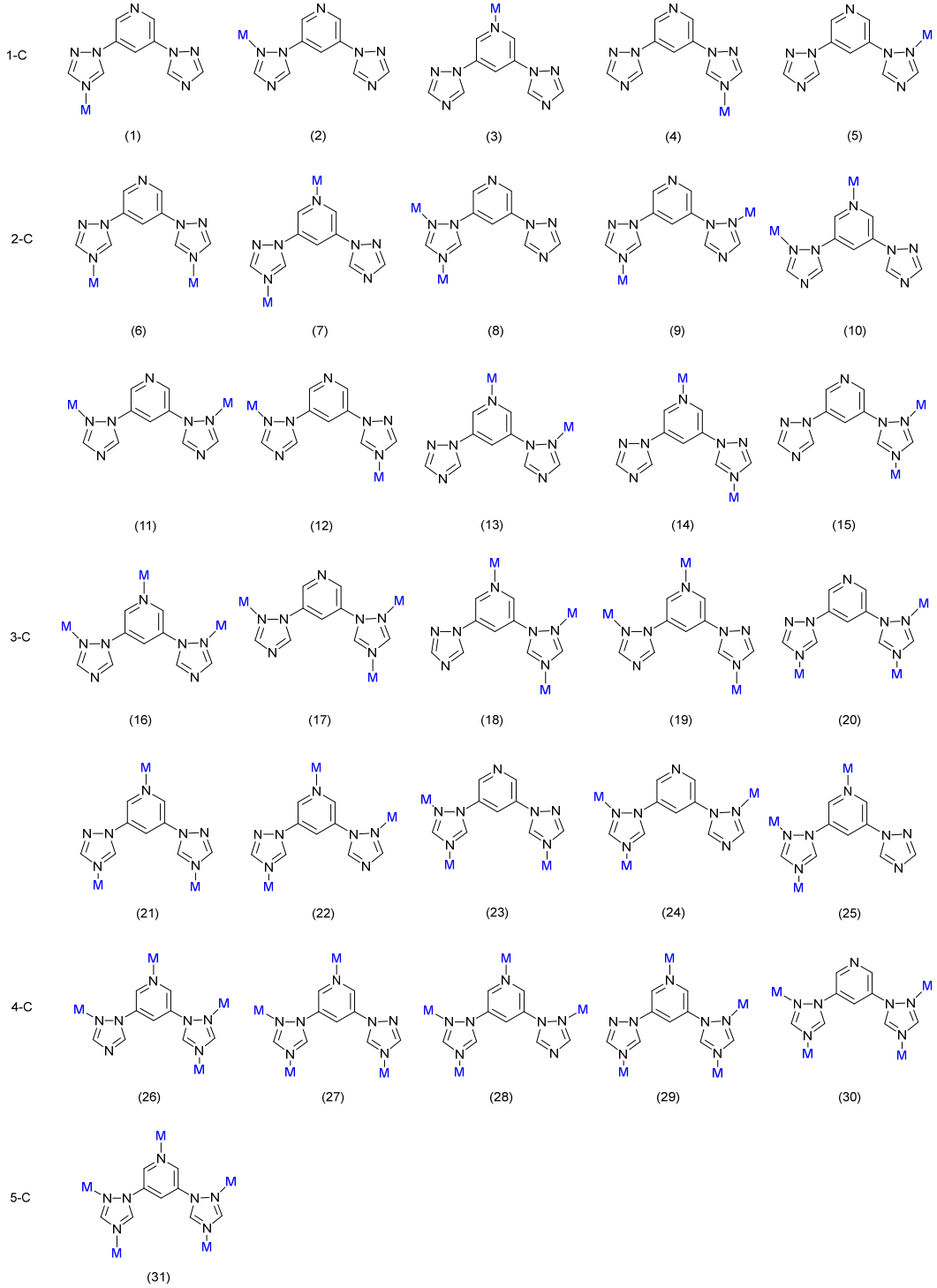


Figure S5: Different coordination modes of 3,5-bis(1’,2’,4’-triazol-1’-yl) pyridine.

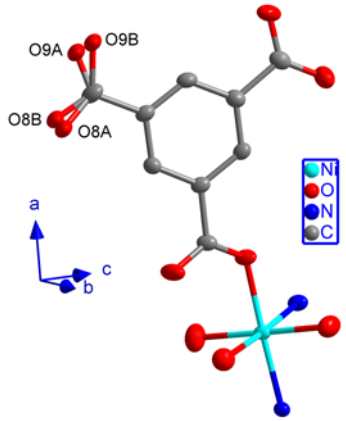


Figure S6: Disorder of O8 and O9 atoms in the Ni(II) coordination polymer.

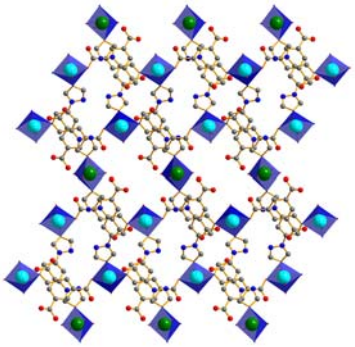

Figure S7: Perspective view of the 2D framework in the Ni(II) coordination polymer along the b axis.

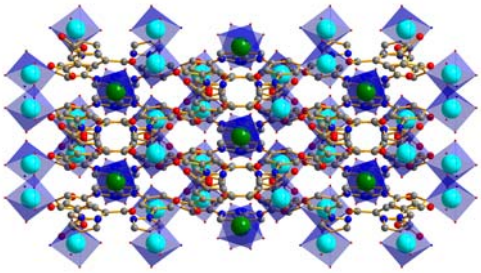

Figure S8: Perspective view of the 2D framework in the Ni(II) coordination polymer along the c axis.

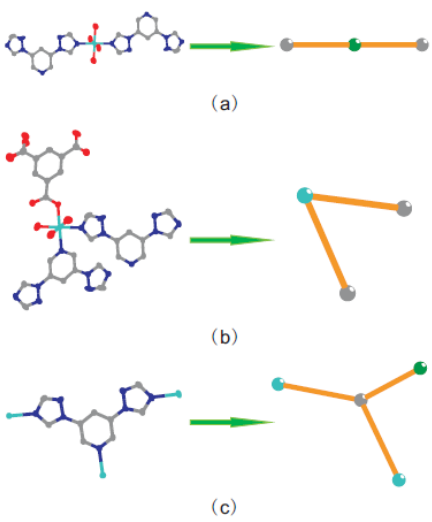


Figure S9: Abstracting the underlying topology in the Ni(II) coordination polymer. (a) Ni(II)1 cations are considered as 2-connected nodes. (b) Ni(II)2-btc motifs are regarded as 2-connected nodes. (c) 3,5-Bis(1',2',4'-triazol-1'-yl) pyridine ligands can be considered as 3-connected nodes. Color code: green ball, 2-connected Ni(II)1 node; light green ball, 2-connected Ni(II)2-btc node; grey ball, 3-connected btap node.

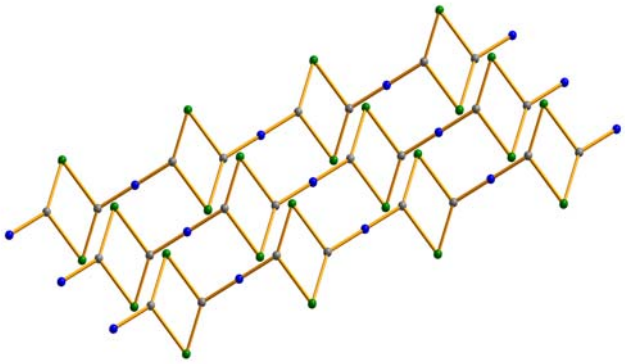

Figure S10: Schematic view of the 3D supramolecular framework of 2. Color code: green ball, 2-connected Ni(II)1 node; light green ball, 2-connected Ni(II)2-btc node; grey ball, 3-connected btap node.

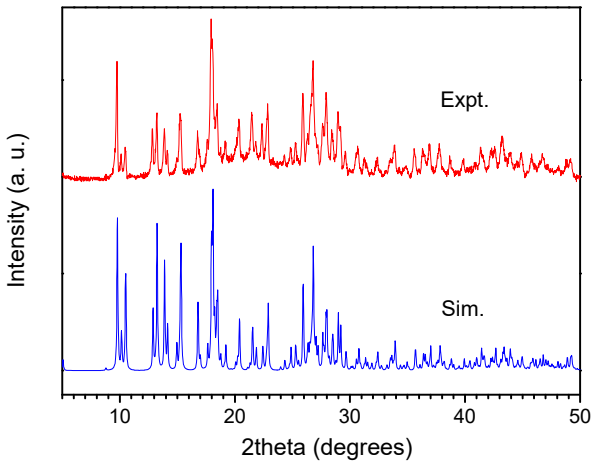


Figure S11: Experimental powder X-ray diffraction pattern for the Ni(II) coordination polymer 2 crystals versus a simulated powder pattern.

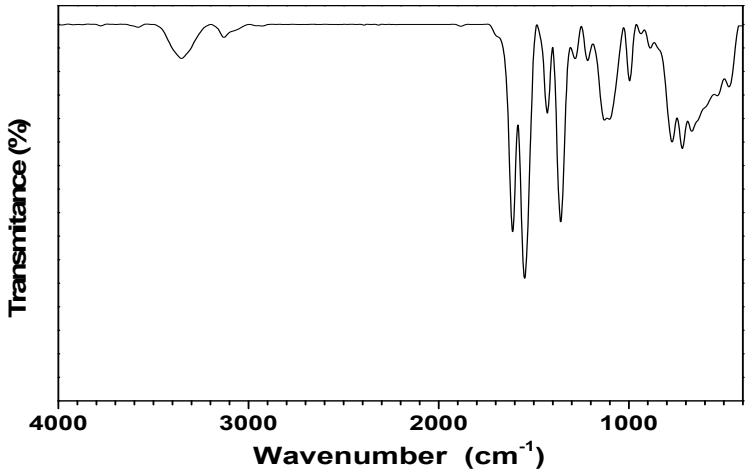


Figure S12: FT-IR spectrum of the Ni(II) coordination polymer **2**.

FT-IR (KBr pellet, $cm^{-1}$): 3353 (w), 3129 (w), 1611 (s), 1548 (s), 1428 (m), 1358 (s), 1282 (w), 1217 (w), 1128 (m), 996 (w), 772 (m), 719 (m), 669 (m). The absence of bands at about 1700 $cm^{-1}$ in Ni-CP indicated the complete deprotonation of aromatic multicarboxylate, which was well matched with the single crystal X-ray analysis. In addition, the weak broad band at 3200-3500 $cm^{-1}$ should be attributed to the vibration of ν(OH) of water molecules.

.

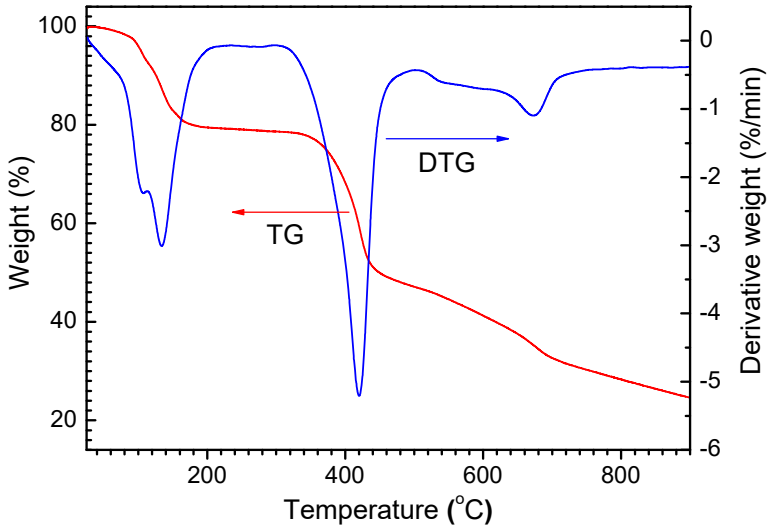


Figure S13: TG and DTG curves of the Ni(II) coordination polymer **2**.

The initial mass loss of Ni-CP occurred in the range of 80-100℃ was attributed to the release of lattice water molecules, and mass loss in the range of 110 - 300℃ was due to the evaporation of coordination water molecules. As the temperature increased from 350 to 900℃, the ligands showed a dominant mass loss owing to the complete decomposition of Ni-CP to nickel oxide. This feature demonstrated that the Ni-CP material had a good thermal stability until 300℃.

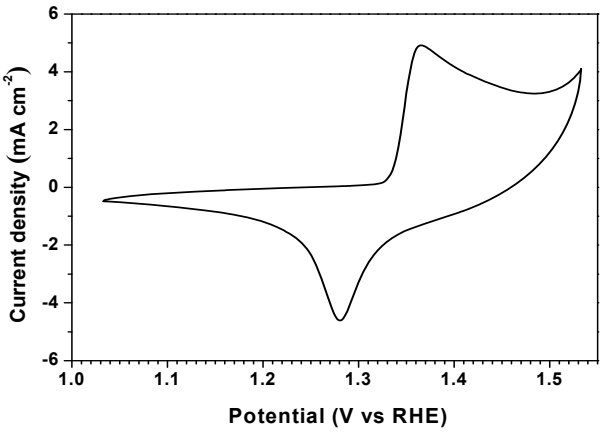


Figure S14: Cyclic voltammetry (CV) curve recorded on the Ni-CP/C 1: 2 sample at a scan rate of 20 mV $s^{-1}$ in 1.0 M KOH solution.

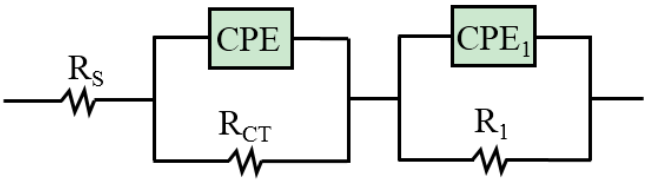


Figure S15: The equivalent circuit of EIS for simulation.

$R_s$ for the uncompensated solution resistance;
$R_{ct}$ interfacial charge transfer resistance;
$R_1$ interfacial resistance;
CPE and $CPE_1$ for the double layer charge capacitance.

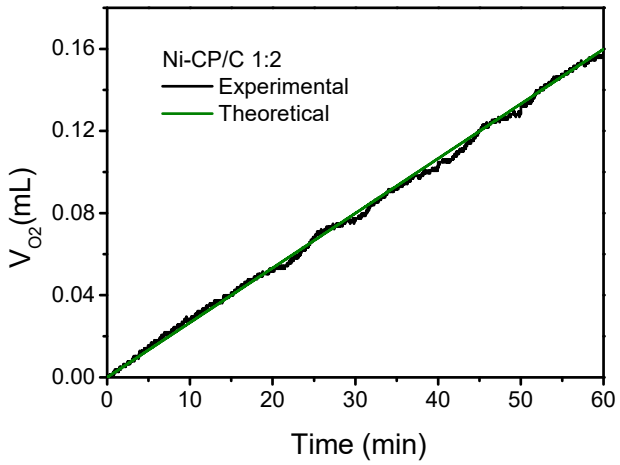


Figure S16: Current efficiency for OER measure at 1.59 V in 1 M KOH for one hour.

The theoretical line represents the ideal amounts of $O_2$ assuming a quantitative of 100% Faradaic yield. The measured $O_2$ line represents the detected $O_2$ during the experiment.

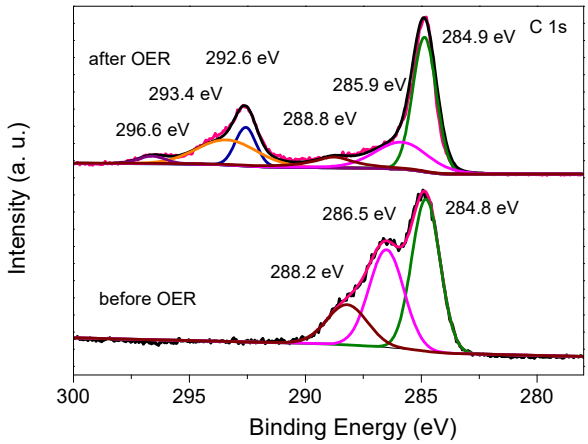


Figure S17: The high-resolution C 1s XPS spectra of Ni-CP/C 1: 2 before and after OER electrolysis.

The peak at 288.2 eV corresponds to the O=C-O, while the peak at 286.5 eV is related to the aryl carbons [20]. The new peaks of 292.6, 293.4, and 296.6 eV can be assigned to C-$F_x$ [21, 22] from the Nafion binder.

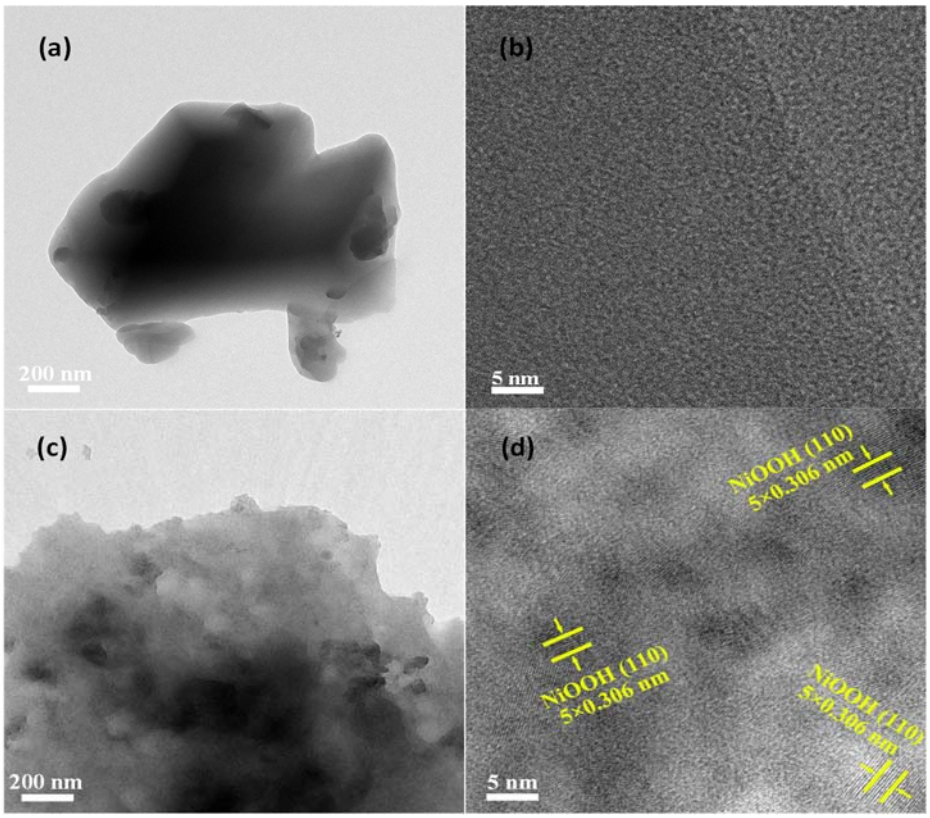


Figure S18 (a, b) TEM and HRTEM images of Ni-CP/C 1: 2 before OER test. (c-d) HRTEM images of Ni-CP/C 1: 2 after OER test.

After the stability test, novel fringe lattice with the interplanar spacing of d(110) = 0.306 nm can be attributed to NiOOH .

References

[1] Bruker Analytical X-ray Systems, Inc., Madison, WI, SMART & SAINT Software Reference Manuals, 6th Edition (2003).

[2] G. M. Sheldrick, SADABS: Software for EmpiricaAbsorption Correction, University of Göttingen, 2nd Edition (2002).

[3] G. M. Sheldrick, SHELXTL, Bruker Analytical X-ray Systems, Inc., Madison, WI, 6th Edition (2001).

[4] Bruker Analytical X-ray Systems, Inc., Madison, WI, SHELXTL Reference Manual, 6th Edition (2000).

[5] G. M. Sheldrick, SHELXT-Integrated space-group and crystalstructure determination, Acta Crystallogr., Sect. A 71 (1) (2015) 3-8.

[6] G. M. Sheldrick, Crystal structure refinement with SHELXL, Acta Crystallogr., Sect. C 71 (1) (2015) 3-8.

[7] P. Müller, R. Herbst-Irmer, A. L. Spek, T. R. Schneider, M. R. Sawaya, Crystal Structure Refinement: A Crystallographer's Guide to SHELXL, Oxford University Press, 2006.

[8] O. V. Dolomanov, L. J. Bourhis, R. J. Gildea, J. A. K. Howard, H. Puschmann, OLEX2: a complete structure solution, refinement and analysis program, J. Appl. Crystallogr. 42 (2) (2009) 339-341.

[9] A. L. Spek, PLATON SQUEEZE: a tool for the calculation of the disordered solvent contribution to the calculated structure factors, Acta Crystallogr., Sect. C 71 (1) (2015) 9-18.

[10] A. L. Spek, Structure validation in chemical crystallography, Acta Crystallogr., Sect. D 65 (2) (2009) 148-155.

[11] V. A. Blatov, A. P. Shevchenko, D. M. Proserpio, Applied topological analysis of crystal structures with the program package ToposPro, Cryst. Growth Des. 14 (7) (2014) 3576-3586.

[12] K. Bradenburg, Diamond, Crystal Impact GbR, Bonn, version 3.1em Edition (2005).

[13] L. Wang, Y. Wu, R. Cao, L. Ren, M. Chen, X. Feng, J. Zhou, B. Wang, Fe/Ni metal-organic frameworks and their binder-free thin films for efficient oxygen evolution with low overpotential, ACS Appl. Mater. Interfaces 8 (26) (2016) 16736-16743.

[14] J. Duan, S. Chen, C. Zhao, Ultrathin metal-organic framework array for efficient electrocatalytic water splitting, Nat. Commun. 8 (2017) 15341. doi:10.1038/ncomms15341.

[15] S. Wang, Y. Hou, S. Lin, X. Wang, Water oxidation electrocatalysis by a zeolitic imidazolate framework, Nanoscale 6 (2014) 9930-9934.

[16] X.-F. Lu, P.-Q. Liao, J.-W. Wang, J.-X. Wu, X.-W. Chen, C.-T. He, J.-P. Zhang, G.-R. Li, X.-M. Chen, An alkaline-stable, metal hydroxide mimicking metal-organic framework for efficient electrocatalytic oxygen evolution, J. Am. Chem. Soc. 138 (27) (2016) 8336-8339.

[17] Y. Gong, H.-F. Shi, Z. Hao, J.-L. Sun, J.-H. Lin, Two novel Co(II) coordination polymers based on 1,4-bis(3-pyridylaminomethyl)benzene as electrocatalysts for oxygen evolution from water, Dalton Trans. 42(2013) 12252-12259.

[18] X.-L. Wang, L.-Z. Dong, M. Qiao, Y.-J. Tang, J. Liu, Y. Li, S.-L. Li, J.-X. Su, Y.-Q. Lan, Exploring the performance improvement of the oxygen evolution reaction in a stable bimetal|organic framework system, Angew. Chem. Int. Ed. 57 (31) (2018) 9660-9664.

[19] J. Jiang, L. Huang, X. Liu, L. Ai, Bioinspired cobalt-citrate metal-organic framework as an efficient electrocatalyst for water oxidation, ACS Appl. Mater. Interfaces 9 (8) (2017) 7193-7201.

[20] L. Ren, F. Yang, C. Wang, Y. Li, H. Liu, Z. Tu, L. Zhang, Z. Liu, J. Gao, C. Xu, Plasma synthesis of oxidized graphene foam supporting Pd nanoparticles as a new catalyst for one-pot synthesis of dibenzyls, RSC Adv. 4 (2014) 63048-63054.

[21] M. Yi, Z. Shen, X. Zhang, S. Ma, Achieving concentrated grapheme dispersions in

water/acetone mixtures by the strategy of tailoring Hansen solubility parameters, J. Phys. D: Appl. Phys. 46 (2) (2013) 025301.
[22] C. Li, X. Hu, W. Tong, W. Yan, X. Lou, M. Shen, B. Hu, Ultrathin manganese-based metal-organic framework nanosheets: Low-cost and energy-dense lithium storage anodes with the coexistence of metal and ligand redox activities, ACS Appl. Mater. Interfaces 9 (35) (2017) 29829-29838.